Earth Radiation Budget: Results of Outgoing Longwave Radiation from *Nimbus-7, NOAA-9,* and ERBS Satellites

T. DALE BESS AND G. LOUIS SMITH

Atmospheric Sciences Division, National Aeronautics and Space Administration/Langley Research Center, Hampton, Virginia

(Manuscript received 27 January 1992, in final form 6 November 1992)

ABSTRACT

Eighteen months of wide field-of-view (WFOV) outgoing longwave radiation (OLR) measurements from the Earth Radiation Budget Experiment (ERBE) *NOAA-9* and *NOAA-10* spacecraft have been deconvolved to produce resolution-enhanced flux maps at the top of the atmosphere. *NOAA-9* had a 0230 LST equator-crossing time, and *NOAA-10* a 0730 LST equator-crossing time. Intercomparison of these results with ERBE scanner and numerical filtered WFOV results is made. Results have also been compared with corresponding months of deconvolved results from the *Nimbus-7* spacecraft (1200 LST equator crossing). Comparisons have been made of zonal profile plots of OLR for the different sensors and of contour maps of differences in OLR between sensors. In general *Nimbus-7* OLR results show reasonable agreement with *NOAA-9* and *NOAA-10* over most regions of the globe. The largest differences occur over the extratropics, noticeably over land and especially over deserts. This study suggests that long-term monitoring of OLR with WFOV sensors is feasible for globally averaged trends to an accuracy of less than 1 W m^{-2}, for the global absolute mean to within 3 W m^{-2}, and for regional monthly means to within 8 W m^{-2} for most of the globe. Global averages for numerical filtered and deconvolved *NOAA-9* WFOV results are consistently higher than *Nimbus-7* deconvolved results because *NOAA-9* results over land and deserts are higher. However, the ERBE *NOAA-9* scanner gives smaller values of OLR over most regions of the globe than either the *NOAA-9* WFOV numerical filtered or WFOV deconvolved results.

1. Introduction

The radiation balance of the earth as observed by earth-orbiting satellites has been of interest to atmospheric scientists since the mid-1960s. Most of these satellites moved in polar, sun-synchronous orbits that allowed twice-daily global observations of weather patterns.

In 1975 a major advance in measuring the earth radiation budget was made with the earth radiation budget experiment (ERB) (Smith et al. 1977). This experiment flew separate but nearly identical payloads at two different times on the *Nimbus-6* and *Nimbus-7* satellites. The ERB instrument package on both of these satellites included two earth-viewing wide-field-of-view (WFOV) flat-plate radiometers: one that measured total irradiance (TOT) and the other that measured shortwave (SW) irradiance. The difference of the two is the outgoing longwave radiation (OLR). The WFOV radiometers viewed the earth's entire "disk" from *Nimbus-6* at the 1100-km altitude and from *Nimbus-7* at the 955-km altitude with equator-crossing times near 1200 and 2400 LST. The SW channel had a spectral range of 0.2–3.8 μm, and the TOT channel measured the irradiance from 0.2 to slightly greater than 50 μm. *Nimbus-6* collected usable data from July 1975 through June 1978. *Nimbus-7* collected data from November 1978 through 1990, although data since 1987 have not been processed.

A resolution-enhancement (deconvolution) technique by Smith and Green (1981) has been applied to 12 years of *Nimbus-7* WFOV OLR data extending from June 1975 through October 1987. Results from this 12-year monthly averaged dataset have been described by Bess et al. (1989) and published in atlases by Bess and Smith (1987a,b; 1991).

In 1984, further advances were made with the Earth Radiation Budget Experiment (ERBE) (not to be confused with the earlier Nimbus ERB experiment) (Barkstrom 1984; Barkstrom and Smith 1986). This experiment consists of three satellites, two sun-synchronous National Oceanic and Atmospheric Administration (NOAA) polar orbiters, and one precessing orbiter, the earth radiation budget satellite (ERBS), that observes at varying local times. The ERBE instrument package on these satellites included earth-viewing narrow-field-of-view (NFOV) scanners as well as nonscanner WFOV active-cavity radiometers with different detectors and filters, but nearly the same viewing geometry as the WFOV flat-plate radiometers on the earlier Nimbus ERB experiment. The major difference in the polar orbiters from the ERB experiment and ERBE is that the ERBE polar orbiters, *NOAA-9* and *NOAA-10,* had different equator-crossing times (0230 and 0730 LST, respectively) and are in a lower orbit (870 km).

Corresponding author address: T. Dale Bess, Langley Research Center, NASA/ASD, Mail Stop 420, Hampton, VA 23681-0001.

The ERBS was launched 5 October 1984, but the first archived data were for November 1984. The coarse spatial resolution WFOV instrument on the ERBS continues to collect data although its high-spatial-resolution scanner failed 28 February 1990, after 64 months of successful operation. The *NOAA-9* satellite was launched 12 December 1984, and the first archived data were for February 1985. The *NOAA-9* scanner failed 21 January 1987, after two years of successful operation. The *NOAA-9* WFOV instrument continues to collect data. The *NOAA-10* satellite was launched on 12 September 1986, and the first archived data were for November 1986. The *NOAA-10* scanner failed on 22 May 1989, after 31 months of successful operation. The *NOAA-10* WFOV instrument continues to collect data. Thus, with the combined WFOV datasets from ERBE and the ERB experiment, there is a 15-yr continuous time series of OLR data available for climate studies. There is also a 3-yr data overlap available between ERB and ERBE, which is very valuable for comparison purposes between the two datasets.

Two papers have recently appeared on the comparison of ERBE data. One focused on intercomparison of scanner and nonscanner measurements from ERBE (Green et al. 1990), and the other on the comparison of ERBE results with *Nimbus-7* results (Kyle et al. 1990).

Most of the results from Kyle et al. pertaining to OLR use WFOV shape-factor results from *Nimbus-7* to compare with ERBE WFOV and scanner time–space-averaged results. Included in their paper are monthly averaged shape-factor results for the months of April, July, and October 1985 and January 1986, but resolution-enhanced (deconvolved) results were presented for only one month, April 1985. Their analysis shows that *Nimbus-7* shape-factor longwave WFOV results agree rather well on a global scale with ERBE scanner results. This good agreement does not carry over to zonal and regional results. Zonal differences of 15 W m^{-2} between shape-factor and scanner results are common, and regional differences exceeding 30 W m^{-2} occur. Largest differences occur in the tropics and midlatitudes. They report that the most important difference arises due to the marked difference in spatial resolution.

The purpose of this paper is to 1) determine spherical harmonic deconvolved results for 18 months of ERBE WFOV-emitted radiation from the *NOAA-9* and *NOAA-10* polar-orbiting satellites; 2) show differences between deconvolved OLR measurements from *NOAA-9* and *Nimbus-7* satellites on global, zonal, and regional scales for the months during which measurements of the two satellites overlapped; 3) compare numerical-filtered measurements and deconvolved measurements with scanner measurements; and 4) determine diurnal variability of OLR.

Spherical harmonics are a natural choice for working with WFOV OLR data when one has the global coverage of polar-orbiting satellites. Spherical harmonics offer higher spatial resolution than the shape-factor technique. Higher resolution is desirable when studying variability of OLR, especially in the tropics and midlatitudes in that zonal profiles of OLR are a little better defined and much of the variance can be represented by a few zonal coefficients, the time series of which are useful in themselves (Auer and Kao 1991). With spherical harmonics, one can represent large datasets with a few coefficients. The mathematical structure of spherical harmonics permits one to separately study latitudinal variations using zonal coefficients and longitudinal variations and wave properties using tesseral coefficients. Also, there is a 12-yr time series of *Nimbus-6 and Nimbus-7* WFOV OLR covering the period from July 1975 to October 1987 that has been analyzed using spherical harmonics to generate monthly mean harmonic coefficients. Thus, using spherical harmonics to represent ERBE WFOV data as they become available is the best way to extend the time series record.

Section 2 of this paper describes the data, its source, and form. Section 3 describes the procedure used to analyze and intercompare the different datasets. Section 4 gives results from the analysis, section 5 a discussion of results, and section 6 the conclusions.

2. Data

From the ERBE experiment, monthly averaged OLR data from the nonscanner aboard the *NOAA-9* and *NOAA-10* polar-orbiter satellites are used. Seventeen months of data from *NOAA-9* have been processed. This includes 5 months from 1985, 11 months from 1986, and 1 month from 1987. Only 1 month (July 1987) from *NOAA-10* is used. All nonscanner measurements are taken from the medium- to wide-field-of-view monthly data tape from the ERBE processing system. These tapes, referred to as S-7, contain only instantaneous nonscanner data. The WFOV data are in three forms: longwave and shortwave flux measurements taken at 4-s intervals at satellite altitude; top-of-the-atmosphere (TOA) longwave and shortwave taken at 16-s intervals using the numerical-filtered technique (Green 1983; Smith et al. 1986); and TOA longwave and shortwave taken at 16-s intervals using the shape-factor technique (Smith et al. 1986). In addition to the nonscanner S-7 data, time–space-averaged scanner OLR data from the S-9 scanner data tapes were used.

From the ERB experiment, WFOV nonscanner measurements from *Nimbus-7* were used. The data are from the solar and earth flux data tapes (SEFDT) supplied by the *Nimbus-7* project. Similar to the S-7 data tapes, the SEFDT tapes have longwave and shortwave flux measurements taken at 4-s intervals at satellite altitude.

Selected months of processed data are used to compare S-7 WFOV results from *NOAA-9* with those of

SEFDT WFOV results from *Nimbus-7*. Also, comparisons of time–space-averaged monthly scanner results from the S-9 data tapes and time–space-averaged monthly nonscanner results from the S-7 data tapes were made on global, zonal, and regional regions.

3. Analysis procedure

The longwave flux at satellite altitude uses all available data, but the numerical filtered longwave processes a sequence of data and cannot use measurements near the terminator. The S-7 tapes were processed by taking all measurements and averaging over 1 month and 5° increments in latitude, forming an igloo-type grid system of near-equal-area regions (Bess and Smith 1987a,b). The igloo grid system is symmetrical about the equator and has three polar regions from 85° to 90° latitude and 72 regions at the equator from 0° to 5° latitude, with a total of 1654 regions over the globe. Data from the *Nimbus-7* SEFDT tapes and the S-9 scanner tapes were gridded in the same manner. However, the S-9 scanner data have initially been gridded into 2.5° × 2.5° equal angular grids, so they were also regridded into 1654 near-equal-area grids. The WFOV numerical-filtered data from S-7 and scanner TOA fluxes from S-9 were then expressed in a series of trun-

July 1986

C_n^m / S_n^m

n/m	0	12	11	10	9	8	7	6	5	4	3	2	1	m/n
0	238.867	-.378	-.154	-.096	-.135	.345	.105	.217	-.536	-.170	-.454	-.858	-.256	12
1	14.115	6.555	.476	-.222	.013	.096	-.107	-.856	.373	1.458	-.126	.153	-.051	11
2	-21.870	4.710	3.518	.104	-.817	.596	.103	.036	1.147	.960	.907	1.656	1.757	10
3	8.423	-.646	2.386	-.067	.068	1.312	.194	.017	-.691	-.098	1.711	2.134	-.417	9
4	-7.899	-1.486	-1.486	-1.200	-4.148	.322	.341	.303	-1.030	-.782	-.688	-.590	-.361	8
5	-4.473	-3.606	-2.934	-.600	-2.674	-1.203	.597	.342	.784	-.478	-2.327	-3.138	.612	7
6	4.101	-.860	-.967	1.926	-.040	.589	1.587	-1.148	-1.419	-.340	-.116	-.210	1.200	6
7	8.429	1.613	-.244	.806	.903	.446	.603	.724	-2.295	-1.123	2.223	-.178	-4.008	5
8	-4.101	.611	1.390	-1.728	.790	-.417	.831	.760	.909	-.416	1.242	.360	3.019	4
9	-4.451	.748	1.392	.263	.240	-.835	-.271	-.538	.475	-.672	-.092	2.909	3.643	3
10	-.006	.045	-.076	2.151	-.545	.494	-.316	.191	-.392	.027	.178	5.642	.068	2
11	1.033	-1.717	-2.478	.416	-.867	.605	-.021	.456	.146	-.847	.088	-.359	-2.201	1
12	1.096	.604	-.597	-.592	-.028	-.150	-.173	-.292	.441	-.193	.849	-.036	.166	

December 1986

C_n^m / S_n^m

n/m	0	12	11	10	9	8	7	6	5	4	3	2	1	m/n
0	232.206	.090	-.584	-.865	-.988	-.577	-.790	-.108	.218	.521	1.890	.317	-.587	12
1	-7.771	1.058	.080	-.208	.940	.100	-.097	.877	.030	-1.402	.548	-.059	1.151	11
2	-24.014	1.037	-.773	.367	-.583	.262	.753	-.134	.324	-.954	-1.889	.734	2.494	10
3	-2.340	-2.072	2.556	4.481	.231	-.829	.103	-1.131	-.113	3.235	.493	.789	-2.634	9
4	-4.217	-.042	3.874	-3.340	.523	-.429	-.299	.549	-1.103	-.551	1.639	-1.017	-.952	8
5	4.638	1.077	.693	-2.754	-1.259	1.332	-.652	-.046	.690	-3.405	-1.559	.668	3.114	7
6	6.663	.899	-.842	4.962	.862	-.579	-.825	-.067	.534	1.31~	-.112	2.951	1.946	6
7	-2.234	-1.312	-.084	1.642	-.138	-.161	1.086	.971	-2.648	1.654	1.809	-.590	-3.195	5
8	-5.159	-1.940	.945	-3.101	-1.271	.278	.939	-.274	.823	-.192	-1.060	-1.793	.666	4
9	1.914	1.631	.272	-1.080	1.051	-.177	-1.105	-.818	.938	1.614	1.160	1.866	.323	3
10	2.575	.999	1.303	.328	1.786	-.318	-.650	.004	-1.962	.457	-.810	1.330	-.700	2
11	.074	-1.410	.164	.508	-.839	-.311	.859	1.071	.310	-.383	1.164	.093	-1.030	1
12	-.221	-.057	-.895	1.472	-.902	.103	.285	.199	.441	.242	-.927	.446	.012	

FIG. 1. Spherical harmonic coefficients of deconvolved *NOAA-9* WFOV OLR.

cated spherical harmonic coefficients for representing OLR results. However, the S-7 WFOV longwave measurements at satellite altitude had to be enhanced after they were time- and space-averaged into regional monthly measurements. The resolution-enhancement (deconvolution) technique was applied to represent the OLR at the TOA by a truncated series of spherical harmonics (Smith and Green 1981). The deconvolution technique takes advantage of the fact that spherical harmonics are the eigenfunctions of the measurement operator and reduces the radiant flux from satellite altitude to TOA by dividing by the appropriate eigenvalues.

The governing equation from which the monthly averaged values of OLR at TOA and any location may be produced by the set of spherical-harmonic coefficients is

$$M(\theta, \phi, t) = \sum_{n=0}^{N} \sum_{m=0}^{n} N_n^m P_n^m(\cos\theta)[C_n^m(t)\cos(m\phi) + S_n^m(t)\sin(m\phi)],$$

where $M(\theta, \phi, t)$ is the OLR at TOA, θ is the colatitude, f is longitude, t is time, and P_n^m are the associated Legendre polynomials of degree n and order m. The terms $C_n^m(t)$ and $S_n^m(t)$ are the cosine and sine real spherical harmonic coefficients, and the normalizing factor is

$$N_n^m = \left[\frac{(2n+1)(n-m)!(2-\delta_0^m)}{(n+m)!}\right]^{1/2},$$

where δ_0^m is the Kronecker delta function.

4. Results

The OLR results in the form of spherical harmonic-tables for July 1986 and December 1986 for the *NOAA-9* WFOV data are shown in Fig. 1. The tables have the same format as those documented by Bess and Smith (1987a,b). Each table contains a set of spherical harmonic coefficients for one month of mean values that can be used to reconstruct the radiation field of the original dataset with relatively few parameters. Results are for a spherical harmonic expansion truncated to the 12th degree. For such a 12th-degree expansion, 169 coefficients are required to specify the radiation field. The format of the tables makes it very easy to select any coefficient. The superscript m is the longitudinal wavenumber or order, and n represents the degree of the spherical harmonic. Thus, in the first column, which represents the zonal terms, m is 0 and n ranges from 0 to 12. The coefficients above the stair-step line are the 78 sine terms. With the exception of the first column, the coefficients below the stair-step line are the 78 cosine terms. The first column on the

	Feb '85	Apr '85	Jly '85	Oct '85	Dec '85	Jan '86	Feb '86	Mar '86	Apr '86	May '86	Jun '86	Jly '86	Aug '86	Spt '86	Nov '86	Dec '86	Jly '87	* Jly '87
C00	236.352	236.895	240.259	235.549	231.591	233.665	233.609	233.653	233.584	235.593	237.517	238.597	238.594	236.531	231.430	232.206	239.900	234.754
C01	-6.974	1.176	14.682	4.259	-7.555	-8.273	-6.889	-3.007	1.047	5.870	10.810	14.115	12.106	8.404	-3.574	-7.771	13.638	12.749
C02	-26.040	-23.636	-21.204	-24.788	-23.521	-24.711	-25.431	-24.851	-23.661	-23.636	-21.739	-21.870	-22.241	-23.511	-23.938	-24.014	-22.711	-22.111
C03	-2.954	2.530	9.087	2.682	-1.868	-3.966	-2.892	-0.377	2.664	5.896	8.335	8.423	8.220	6.850	0.309	-2.340	8.769	10.003
C04	-4.348	-7.451	-8.589	-7.121	-3.490	-4.307	-3.303	-6.802	-7.085	-5.650	-7.226	-7.899	-8.464	-9.087	-4.799	-4.217	-6.536	-6.476
C05	8.994	2.615	-3.766	-0.073	5.100	7.198	7.297	5.922	3.111	-0.875	-2.885	-4.473	-5.787	-4.232	2.081	4.838	-3.646	-3.820
C06	5.775	4.612	4.510	3.785	6.365	7.404	5.118	6.268	4.522	4.339	4.603	4.101	2.523	3.457	6.114	6.663	5.226	4.299
C07	-5.164	-0.403	8.549	4.414	-1.880	-5.107	-5.961	-4.589	-1.983	4.720	7.836	8.429	8.976	6.787	1.786	-2.234	7.595	6.852
C08	-5.943	-5.866	-3.557	-4.214	-5.216	-5.217	-5.999	-8.281	-6.332	-5.881	-5.927	-4.101	-1.398	-3.878	-5.713	-5.159	-5.215	-5.339
C09	3.294	1.170	-3.752	-3.294	1.701	2.819	3.450	3.260	2.649	-1.852	-5.195	-4.451	-4.315	-3.375	-0.567	1.914	-4.882	-4.514
C010	1.642	2.690	0.051	0.983	2.458	1.664	2.140	3.372	3.376	2.315	1.593	-0.006	-0.291	1.532	1.679	2.575	1.062	1.653
C011	-0.437	-0.493	0.319	1.805	-0.080	-0.017	-0.404	0.518	-0.752	1.406	2.726	1.033	0.211	1.991	1.253	0.074	2.298	1.760
C012	0.324	-1.248	0.985	0.424	-0.241	0.229	0.007	-0.339	-1.580	0.305	0.662	1.095	0.700	0.557	0.924	-0.221	0.639	0.258

FIG. 2. Spherical harmonic zonal coefficients for 18 months of WFOV ERBE OLR data. *NOAA-10* data are indicated by the asterisk. The other data are *NOAA-9*.

left contains the 13 zonal terms. The sine and cosine terms represent the nonaxisymmetric terms and give a measure of longitudinal variation. Physical interpretations can be associated with some zonal terms. Thus, C_0^0 is the global average and C_1^0 is a measure of differences in the Northern and Southern hemispheres, as are the other coefficients with odd n. The coefficients with even n measure equator-to-pole gradients with most of the gradient represented by C_2^0. It has been shown that over 80% of the degree variance is in the zonal terms and over 70% are in the first five (excluding C_0^0) terms (Smith and Bess 1983). The high percentage of degree variance in zonal terms is because at large scales, seasonal variation in earth-emitted radiation is strongly dependent on latitude outside the tropics. Because of the importance of the zonal terms at large scales, the table in Fig. 2 is included to show the zonal terms for all 18 months of the *NOAA-9* and *NOAA-10* WFOV ERBE monthly mean values. Plots of coefficients C_1^0–C_4^0 with time are shown in Fig. 3. Both C_1^0 and C_3^0 are sinusoidal with positive biases of 1.8 and 2.5 W m^{-2}, respectively, because of land–ocean distribution differences of the Northern and Southern hemispheres. Here, C_1^0 and C_3^0 show more variation in time than C_2^0 and C_4^0; C_1^0 has a range between minima and maxima of 22 W m^{-2}, whereas C_3^0 has a range between minima and maxima of 13 W m^{-2}. Coefficients C_2^0 and C_4^0 have average values of -23.7 and -6.2 W m^{-2}. They are sinusiodal, but the range between minima and maxima is only about 5 W m^{-2}.

Figure 4 shows an average global contour map of OLR for July 1986 for deconvolved results from the WFOV data from *NOAA-9*. The contour interval is 10 W m^{-2}, and radiation values greater than 240 W m^{-2} are represented by solid contour lines. A map for July 1986 of *Nimbus-7* WFOV deconvolved results shown in Fig. 5 looks very much like the *NOAA-9* map in that the features of both maps are very similar in the general structure of contours and the location of high and low values of OLR. However, there are significant differences, especially over land regions, noticeable in the Arabian desert region, which show up more clearly when one looks at zonal plots of OLR and difference contour maps of the OLR between *NOAA-9* and *Nimbus-7*. Section 5 will discuss the differences between deconvolved *NOAA-9* and *Nimbus-7*.

Figure 6 shows zonal plots of average monthly OLR for four datasets for July 1986. Three of these—scanner, numerical filtered, and deconvolved using spherical harmonics—pertain to *NOAA-9*. The other is the *Nimbus-7* deconvolved results. All results show the best agreement in the Southern Hemisphere tropics and midlatitudes. Numerical-filtered results and deconvolved results from *NOAA-9* agree very well with each other except from 85° to 70°S, where the numerical-filtered data are about 5–20 W m^{-2} larger. *NOAA-9* scanner results agree well with *NOAA-9* deconvolved results from 85°S to 15°N. However, both *NOAA-9*

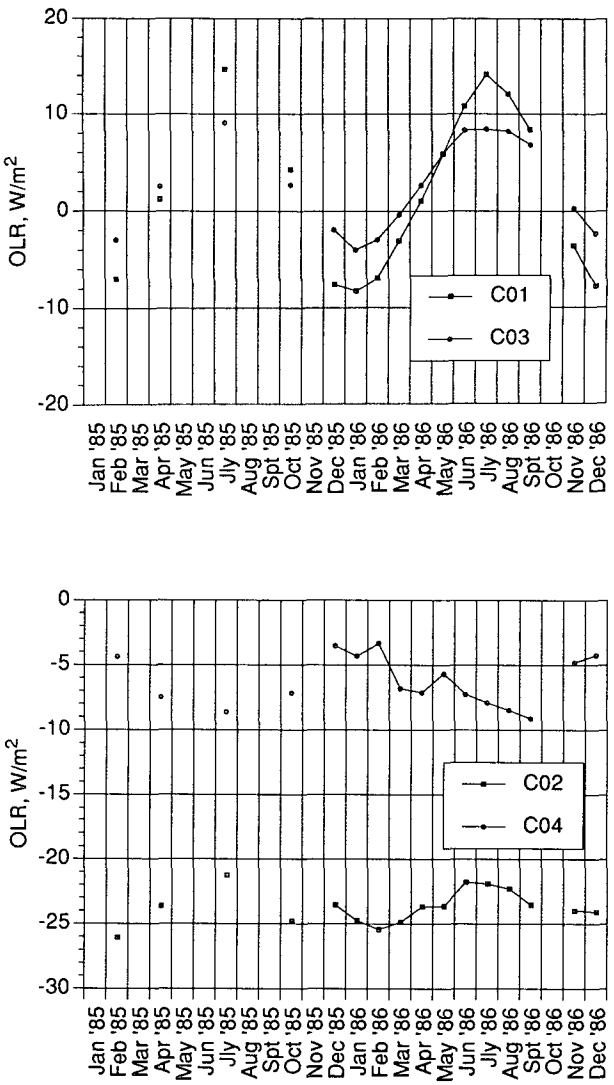

FIG. 3. Zonal coefficients for monthly averaged OLR for *NOAA-9* deconvolved WFOV data.

WFOV deconvolved and WFOV numerical-filtered data are 5–10 W m^{-2} higher than *NOAA-9* scanner data from 15° to 85°N. *Nimbus-7* deconvolved results show reasonably good agreement with *NOAA-9* scanner results from 40°S to 45°N latitude. In the high-latitude regions beyond 45°N and 45°S, *Nimbus-7* is about 5–15 W m^{-2} smaller than scanner values.

Figure 7 shows the same type of zonal plots of average monthly OLR for the *NOAA-9* scanner, numerical-filtered, and deconvolved and the *Nimbus-7* deconvolved datasets for the month of December 1986. The *NOAA-9* scanner is consistently lower than all the other datasets by about 8 to 12 W m^{-2}, especially in the Southern Hemisphere. Agreement is better in most of the Northern Hemisphere. The largest difference between *NOAA-9* deconvolved and *Nimbus-7* decon-

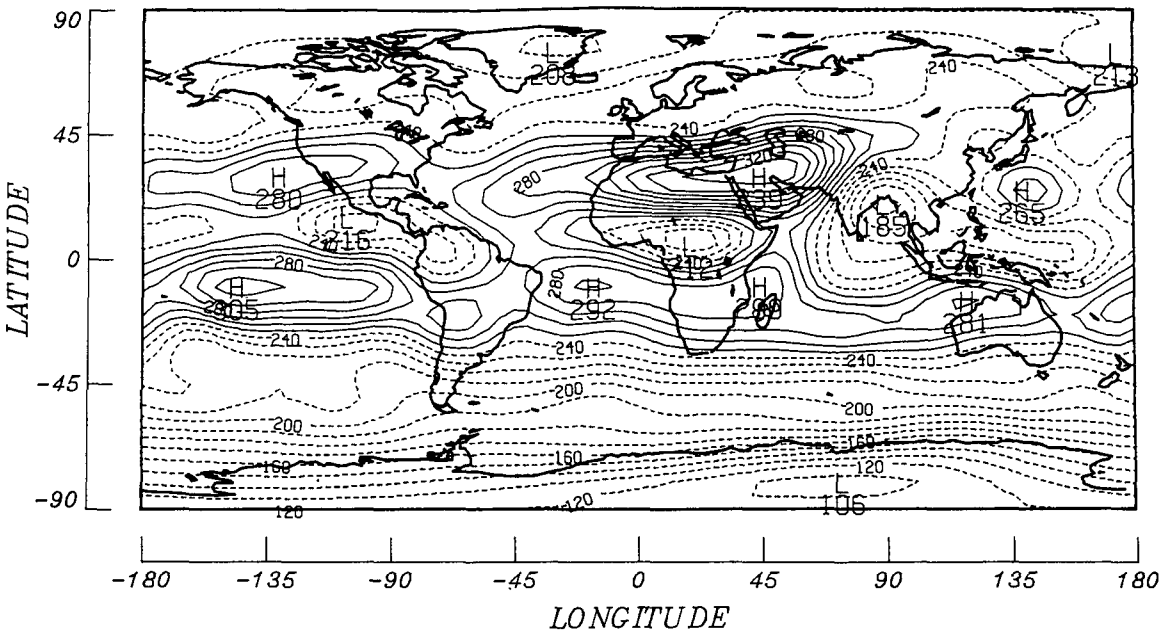

FIG. 4. Average global contour map of OLR deconvolved results from *NOAA-9* WFOV for July 1986.

volved results on a zonal scale is again over the high-latitude regions of the Northern Hemisphere where the maximum is about 10 W m^{-2}.

Figures 8 and 9 show where these differences occur on a regional scale. Figure 8 is a contour map of differences between *NOAA-9* S-7 WFOV OLR data and *Nimbus-7* WFOV averaged OLR data for the month of July 1986. As with Fig. 4, results for both satellites have been resolution enhanced using 12th degree spherical harmonics. The contour interval between contours is 4 W m^{-2}, and dashed lines are minus values meaning that *Nimbus-7* results are larger than *NOAA-9* results in these regions. Highest positive differences are over the desert regions of northern Africa and Saudi

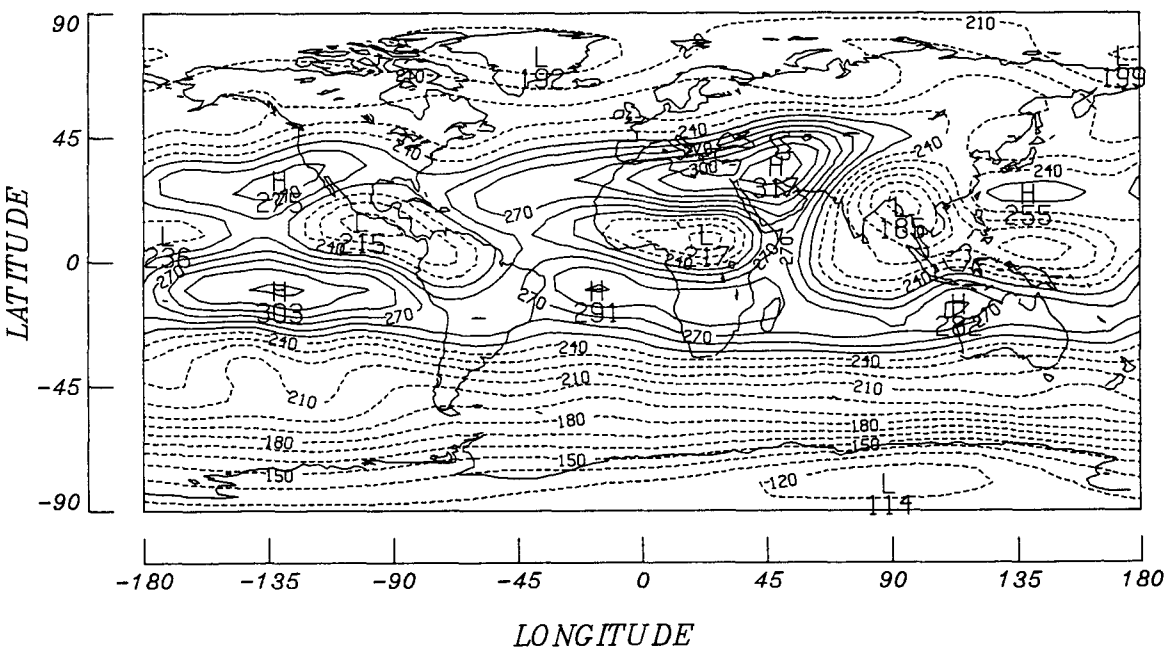

FIG. 5. Average global contour map of OLR deconvolved results from *Nimbus-7* WFOV for July 1986.

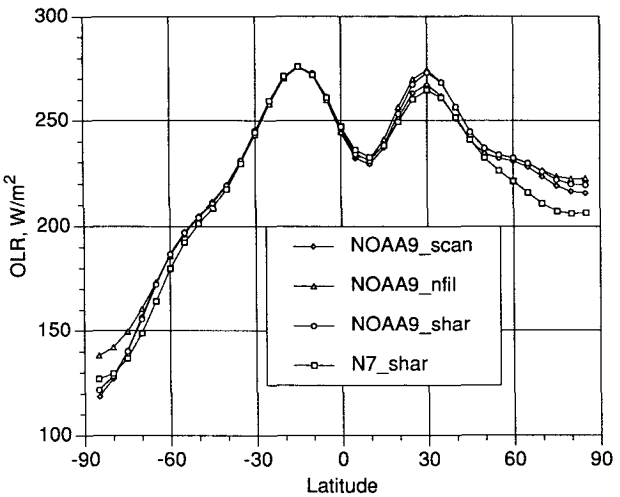

FIG. 6. Zonal average monthly OLR for *NOAA-9* scanner, numerical filtered, spherical harmonic deconvolved, and *Nimbus-7* spherical harmonic deconvolved results for July 1986.

Arabia. The cold, snow-covered, high-latitude regions of Asia, North America, Greenland, and the Arctic region have some reasonably high differences, but the differences are not as significant because of the small areas at these latitudes. The desert regions are characterized by an absence of clouds and low humidity. Other than the desert regions and the high-latitude cold regions of Asia, there are fairly small differences between *NOAA-9* and *Nimbus-7* over most of the regions of the globe. A small difference occurs over southern Russia, that is, the Black, Caspian, and Aral seas. The region is made up of a combination of warm temperate climate and cool dry climate with moderate rainfall and vegetation. Except for the large differences over continental land regions of the Northern Hemisphere, the differences between *NOAA-9* and *Nimbus-7* are generally between 0 and 8 W m^{-2}. Much of the smaller differences are over oceans where *Nimbus-7* results are a little larger than *NOAA-9*. The difference map for August 1986 (not shown) is very similar to July with maximum differences over the northern African deserts, Saudi Arabia, and the high-latitude snow regions. However, the month of March 1986 has large differences of about 20 W m^{-2} over the high-latitude region of Siberia at 60°N, but the difference over the Northern Hemisphere deserts and much of the Southern Hemisphere is much smaller. The difference map for September 1986 is similar to the difference map for March 1986, with the largest difference over Siberia at about 50°N.

Figure 9 for December 1986 shows that the difference between *NOAA-9* and *Nimbus-7* deconvolved results for desert regions and high-latitude regions of the Northern Hemisphere is much smaller than for July 1986. The largest positive difference has shifted south with the seasons to the desert regions of Australia. Other positive highs are located over Central America and just off the coast of Madagascar. OLR from *NOAA-9* is a little larger than OLR from *Nimbus-7* in the Northern Hemisphere mid- and high latitudes and in the southern midlatitudes. *Nimbus-7* OLR is a little larger in the high-latitude regions of the Southern Hemisphere. Again, the largest differences tend to be located over continents.

Figure 10 for July 1986 shows the standard deviation of the OLR with respect to zonal mean OLR at each latitude. The zonal standard deviation ranges from 4 to 34 W m^{-2} over the latitudinal bands. Highest values are at 30°N where *NOAA-9* deconvolved OLR and *NOAA-9* numerical filtered OLR both peak at about 34 W m^{-2}. *Nimbus-7* deconvolved OLR and *NOAA-9* scanner OLR show lower values of standard deviation, being at about 27 and 29 W m^{-2}, respectively. The variation in the tropics and midlatitudes is due to the ocean–land contrast and to the meteorology of the regions in these latitude zones. At 30°N, the variation is due primarily to the contrast between the ocean areas and the hot desert land areas over Central America, Africa, and Asia. In the active monsoon region at 10°N, the zonal standard deviation dips because the contrast between land and oceans is not as great. The peak at 10°S is outside the monsoon region as far as clouds are concerned.

Zonal variation for December 1986 (not shown) shifts with the season such that a maximum of about 30 W m^{-2} is now between 5° and 10°S. Again, the variation is due to the contrast between the heated continental regions and the cooler oceans, and to the winter monsoons (Fein and Stephens 1987).

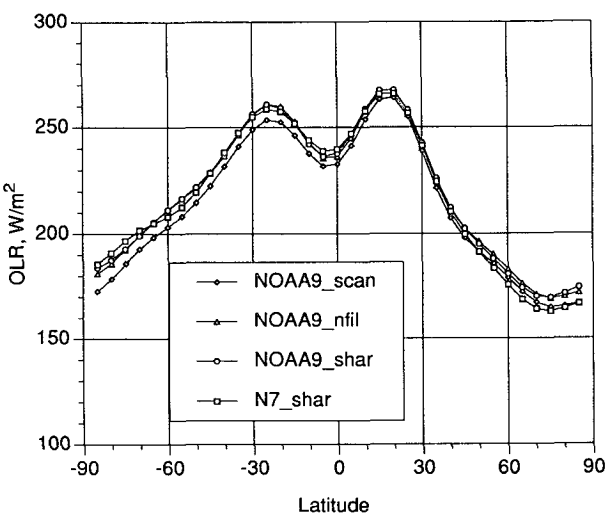

FIG. 7. Zonal average monthly OLR for *NOAA-9* scanner, numerical filtered, spherical harmonic deconvolved, and *Nimbus-7* spherical harmonic deconvolved results for December 1986.

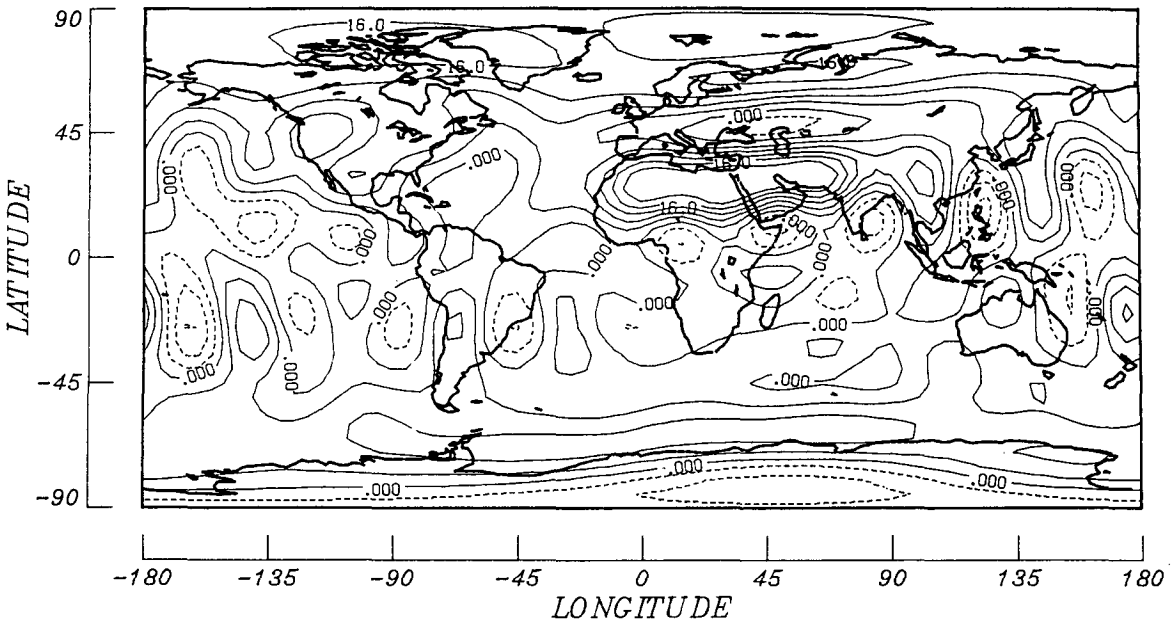

FIG. 8. Contour map of the difference between *NOAA-9* and *Nimbus-7* WFOV averaged OLR for July 1986.

5. Discussion of results

A number of reasons may be given for the difference in OLR measurement, which is determined by differencing the TOT and SW sensors on the *NOAA-9* and *Nimbus-7* satellites. The instruments aboard the two satellites that contain the sensors for measuring total irradiance and shortwave irradiance initially had about the same spectral response, although the instruments are not identical. The WFOV sensors on *Nimbus-7* are flat-plate thermopile detectors. The SW channel is equipped with two fused silica hemispherical domes for charged-particle and infrared attenuation filtering. *NOAA-9* sensors are cavity radiometers, and the SW channel is equipped with only a single-fused silica filter dome. The ages of the sensors are also different since *Nimbus-7* has been flying since 1978 but *NOAA-9* only since 1984. Thus, even if the sensors performed nearly

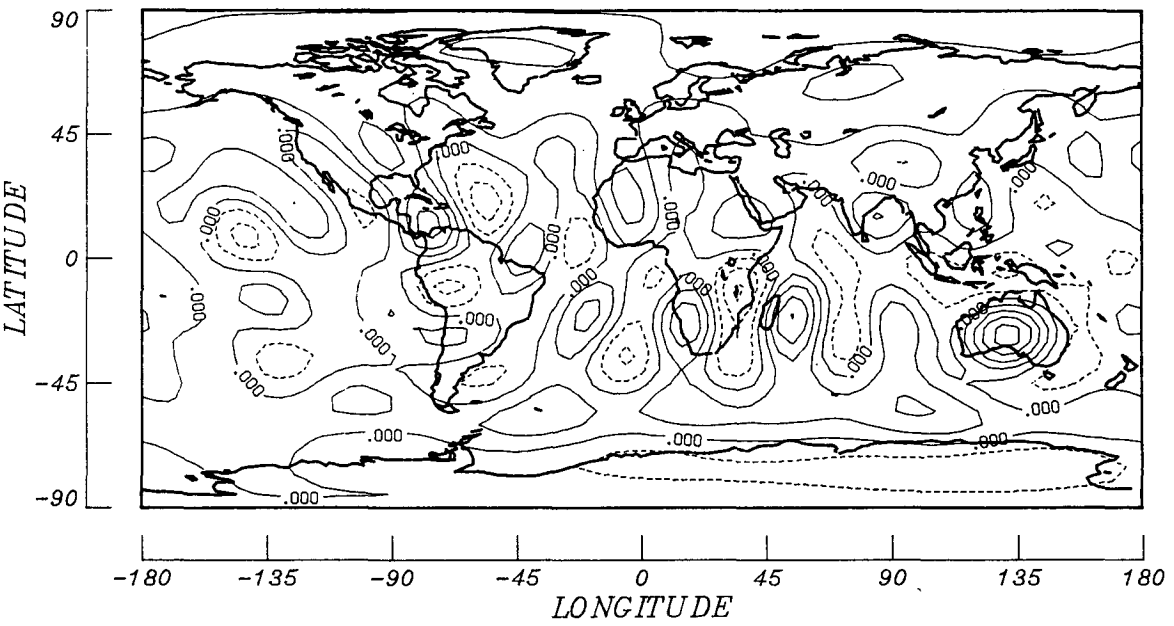

FIG. 9. Contour map of the difference between *NOAA-9* and *Nimbus-7* WFOV averaged OLR for December 1986.

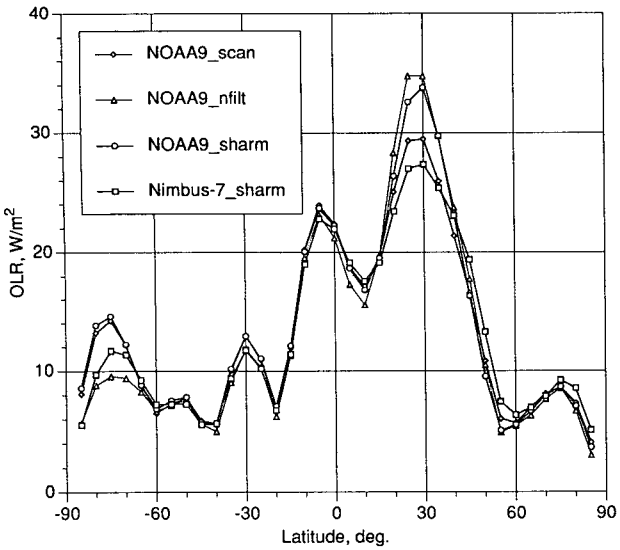

FIG. 10. Zonal variation for *NOAA-9* scanner, numerical filtered, spherical harmonic deconvolved, and *Nimbus-7* spherical harmonic deconvolved results for July 1986.

identically when first flown, degradation of sensor surfaces may be very different for the two satellites. Besides physical and age differences of sensors, one must consider other things such as calibration procedures, temporal sampling strategy, spatial resolution, algorithms used to calculate radiation products, and different altitudes of the two satellites. Another real difference in OLR and SW radiation between *Nimbus-7* and *NOAA-9* is due to the different equator-crossing times of the two satellites of approximately 3 h. For more insight into the differences between *Nimbus-7* and *NOAA-9* and their sensors for measuring radiation, see Jacobowitz et al. (1984) and Barkstrom (1984).

On a global scale, the difference between *NOAA-9* and *Nimbus-7* WFOV deconvolved results is reflected in the monthly global average of OLR. Figure 11 shows time-series plots of global averages of OLR for 16 months of *NOAA-9* and 23 months of *Nimbus-7* WFOV data that were deconvolved using spherical harmonics. No *Nimbus-7* data were taken from 10 April to 23 June 1986, due to other special requirements of the satellite. Thus, there are no data for May 1986, and even April and June are a little questionable and may be somewhat biased. The slope in the trend line between any two neighboring months of the time series for the two datasets are nearly the same, to within about 1 W m^{-2}. This is illustrated in Fig. 12, which plots the difference in global averaged OLR between neighboring months for both *Nimbus-7* and *NOAA-9*. However, *NOAA-9* monthly averages range from 1 to 6.5 W m^{-2} greater than *Nimbus-7* averages. Global averages for February 1985, April 1985, and July 1985 for *NOAA-9* appear to be high when compared to *Nimbus-7* and to the corresponding months in 1986 for *NOAA-9*.

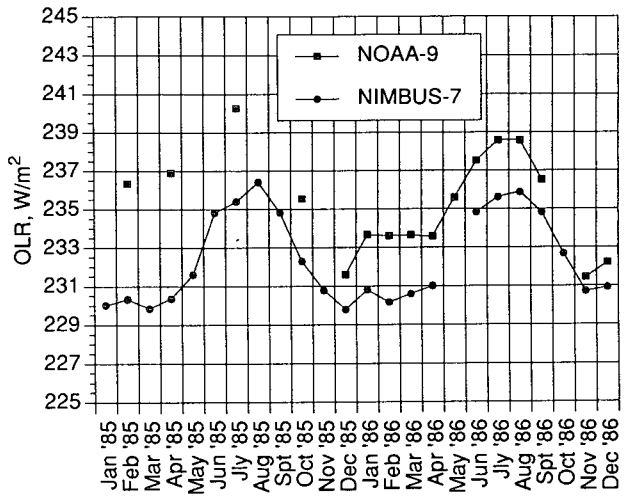

FIG. 11. Global monthly average for *NOAA-9* and *Nimbus-7* WFOV deconvolved results.

As shown in Fig. 8, the largest difference in the regional averages between *Nimbus-7* WFOV and *NOAA-9* WFOV instruments can be attributed to a few land locations that are concentrated mostly over desert regions. Agreement over ocean regions is better. *Nimbus-7* WFOV deconvolved OLR results are consistently lower than ERBE WFOV deconvolved results at the higher-latitude regions of both hemispheres. Kyle et al. (1990) also observed these differences. They suggested that the divergence of the results at these high latitudes may be due to sensor calibration corrections for intraorbital temperature variations near satellite sunrise and sunset for *Nimbus-7*. Of course, the *NOAA-9* ERBE sensor readings may also have errors.

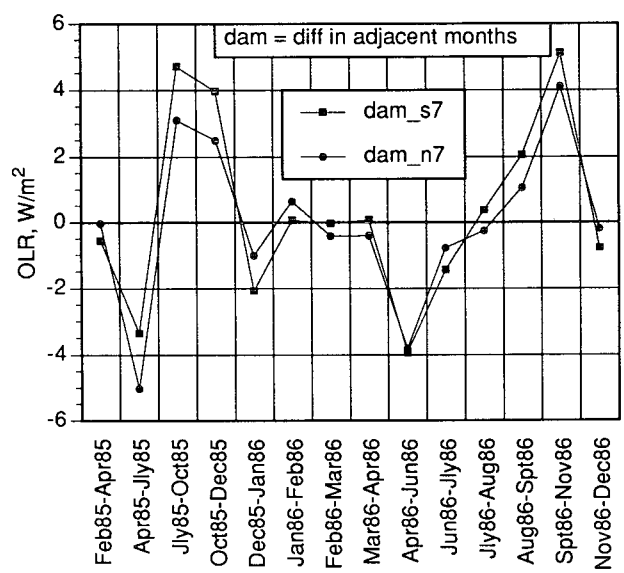

FIG. 12. Difference in global averaged OLR between adjacent months for both *Nimbus-7* and *NOAA-9* WFOV.

Some difference between the *Nimbus-7* and *NOAA-9* WFOV results shown in Fig. 8 should occur because of differences in equator crossing times, which are near 1200 for *Nimbus-7* and 1500 for *NOAA-9*. Figure 8 shows this difference is much too large and in the wrong direction over the Sahara Desert. *Nimbus-7* should show slightly larger values of OLR. To help understand this, Fig. 13 is included. Figure 13 is a map of OLR at 1500 LST minus OLR at 1200 LST as determined from the combined *NOAA-9* ERBS scanner results from the S-9 tapes. It is apparent that the larger differences occur over land, with the maximum at noon. The scanner results show that over the African deserts, the OLR is 6–7 W m^{-2} larger at 1200 than at 1500 LST. This result is in direct contradiction to the comparison of Fig. 8, so that the difference of measurement times does not explain Fig. 8.

Unfiltered WFOV measurements from *Nimbus-7* and *NOAA-9* were treated the same way. The measurements were time- and space-averaged over a month into near-equal-area regions of the globe. Average value regional values were then deconvolved to produce OLR at TOA. Some difference in OLR between *Nimbus-7* and *NOAA-9* occurs over many regions of the globe.

Larger differences occur over the desert regions of Africa in July (and over the desert regions of Australia in December). These large differences are not unique to processing the datasets using deconvolution. The contour map showing the difference between *NOAA-9* and *Nimbus-7* OLR for July 1986 using the shape factor technique gives a very similar result to the difference map in Fig. 8, with the largest difference of 22 W m^{-2} in favor of *NOAA-9* over the desert regions of Saudi Arabia.

Nighttime differences over desert between *NOAA-9* and *Nimbus-7* are in the right direction, with *Nimbus-7* being about 13 W m^{-2} larger than *NOAA-9*. However, for daytime differences, *NOAA-9* is 30 W m^{-2} larger than *Nimbus-7* over the desert region. This result tends to imply that the differences between the two satellites are in the shortwave sensors. If this is the case, then one might suspect that the differences are between the *NOAA-9* active cavity radiometer with its single-fused dome and the *Nimbus-7* flat-plate thermopile detector with its double-fused silica filter dome. Kyle et al. (1990) refer to intraorbital temperature variations and calibration uncertainties being the most probable explanation of the divergence at high latitudes of the WFOV longwave radiation and albedo results between *Nimbus-7* and *NOAA-9*. These same problems may occur over the hot desert regions. Dome heating problems could cause an increase in shortwave radiation that would drive the OLR down.

Some of the difference between *NOAA-9* and *Nimbus-7* may also be related to differences in viewing geometry of the two satellites. *NOAA-9* has an orbit of 870 km, whereas *Nimbus-7* has an orbit altitude of 955 km. Being at a higher altitude, *Nimbus-7* will observe more area of the globe outside the desert regions than *NOAA-9* and will record lower average OLR values. The difference in OLR that occurs between *Nimbus-7* and *NOAA-9* is directly related to the averaged unfiltered measurements for the two satellites. To see this refer to Fig. 14, which is a scatterplot of gridded daytime

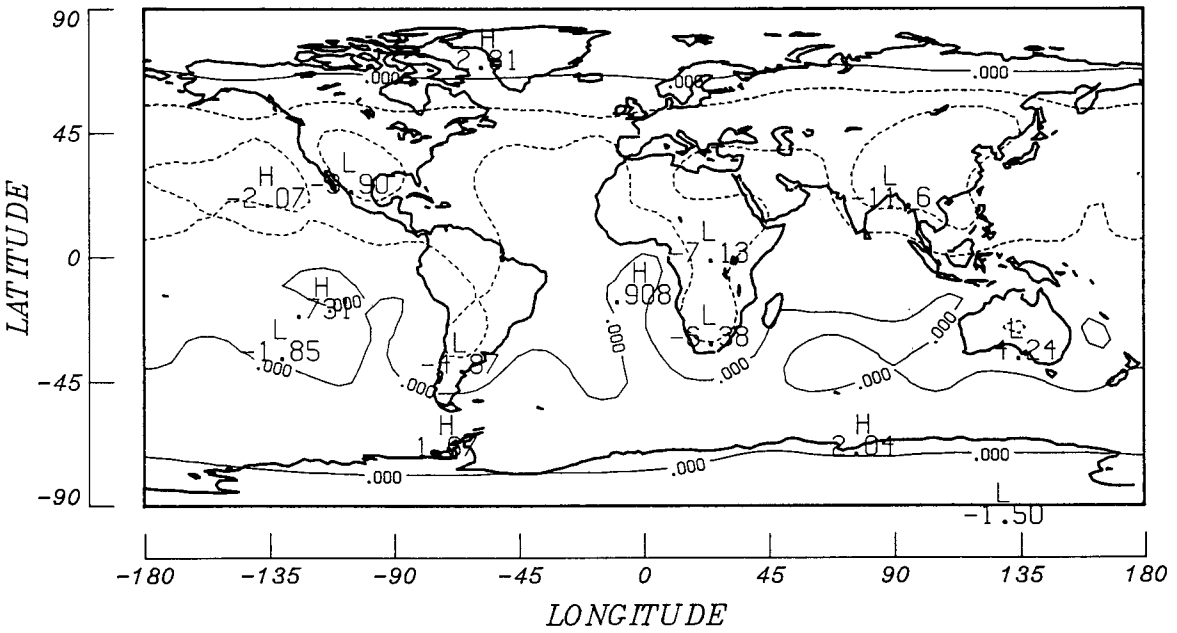

FIG. 13. Difference of OLR between 1500 and 1200 LST for July 1986 from scanner results from combined *NOAA-9* ERBS scanning radiometers.

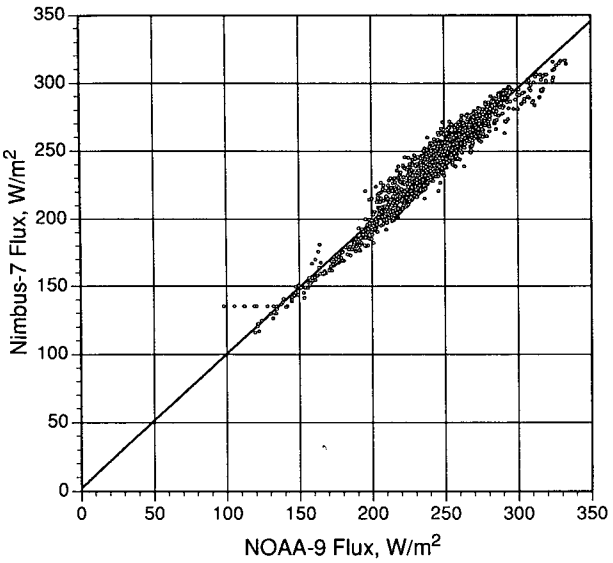

FIG. 14. Gridded daytime WFOV longwave flux values for July 1986 for *NOAA-9* and *Nimbus-7*.

WFOV longwave flux values for *NOAA-9* and *Nimbus-7* for July 1986 at the TOA for all grids of the globe. Between 200 and 300 W m^{-2}, flux values are more uniformly distributed and differences are smaller. Above 300 W m^{-2} (the desert region) *NOAA-9* is 20 to 30 W m^{-2} larger than *Nimbus-7*. Also in the high-latitude regions of the Northern Hemisphere where OLR is less than 200 W m^{-2}, *NOAA-9* flux values are generally higher than *Nimbus-7*. An exception is the latitude band near Australia where *Nimbus-7* is larger.

To understand these differences in regional OLR between *NOAA-9* results and *Nimbus-7* results, differences in total flux and differences in shortwave flux between the WFOV sensors on the two satellites were investigated. Unfiltered measurements at satellite altitude averaged over 16-s intervals were used from 85°N to 60°S to eliminate any problems caused by the sun view angle unique to the WFOV instruments.

If the difference in total flux measurements and the difference in shortwave flux measurements between *Nimbus-7* and *NOAA-9* were consistent at all grid points, then the difference in OLR between the two would at most be small over most regions. Because the differences are not consistent from region to region, some large differences in OLR occur, most notably over desert regions.

It is not clear why the differences in unfiltered measurements are greatest over desert regions, but differences that occur over all regions are likely influenced most by satellite systems having different shortwave sensor design, different calibration procedures, and different algorithms used to calculate radiation products. Because of the differences, some care should be exercised when combining datasets from different satellite systems.

The large difference in OLR between *NOAA-9* and *Nimbus-7* over the desert regions is what one might expect if *Nimbus-7* had an equator-crossing time in the morning near 0700 instead of at 1200 LST. Studies using a diurnal model and fluxes from the combined

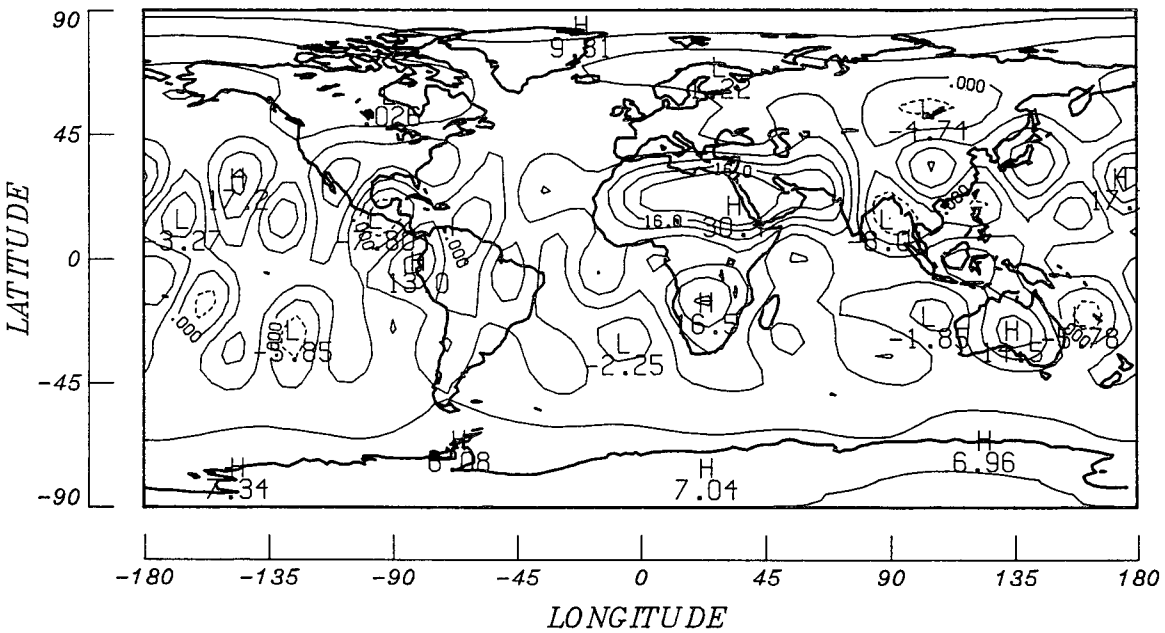

FIG. 15. Diurnal variation of OLR for July 1987 determined from WFOV sensors by differencing results of *NOAA-9* and *NOAA-10* spacecraft.

NOAA-9 ERBS scanners show how these large differences are concentrated over land regions, particularly over desert regions of Africa and Australia where peak values of 30 W m^{-2} can occur (Harrison et al. 1988). Figure 15 is included to demonstrate that diurnal variability can be determined reasonably well from WFOV sensors when direct comparisons can be made between two satellites with different equator-crossing times. Shown is a difference map of deconvolved OLR results between *NOAA-9* and *NOAA-10* WFOV satellite data for July 1987. *NOAA-10* has an equator-crossing time of 0730 LST. Also shown are some large differences over land with a peak of about 30 W m^{-2} over the Sahara; diurnal variability over oceans is low.

6. Conclusions

Outgoing longwave radiation results from the *Nimbus-7* ERB WFOV instruments have been compared with those from the ERBE instruments aboard the *NOAA-9* and *NOAA-10* satellites. In general, *Nimbus-7* OLR results show reasonable agreement, to within 8 W m^{-2}, with *NOAA-9* deconvolved OLR results over most regions of the globe. Regions are of quasi-equal area, with $5° \times 5°$ resolution at the equator. There are larger differences, noticeably at higher latitudes and regions concentrated over land and desert. Although it is difficult to pinpoint the causes of the large differences over desert, results of daytime and nighttime differences suggest that the shortwave channels may be at fault due to their different design for *Nimbus-7* and *NOAA-9*. Some of the difference may also be related to different viewing geometry of the two satellites. In any case the differences are apparent in the monthly averaged unfiltered measurements from the two satellites. Numerical filtered WFOV results compare favorably with WFOV deconvolved results, but degrade a little at high latitudes. Long-term monitoring of OLR with WFOV and scanner instruments is feasible for globally averaged trends to an accuracy of less than 1 W m^{-2}, for the global absolute mean to within 3 W m^{-2}, and for regional monthly means to within 8 W m^{-2} for most regions of the globe. Measurements from WFOV results from *NOAA-9* and *NOAA-10* satellites with different equator-crossing times determine diurnal variability very well.

Acknowledgments. We wish to thank Dr. Lee Kyle and the *Nimbus-7* project for supplying the SEFDT data tapes that contained all of the *Nimbus-7* data. We also thank the ERBE project for all of the *NOAA-9* and *NOAA-10* data.

Nimbus-7 ERB and ERBE data with user's guide are available to the scientific community through the National Space Science Data Center (NSSDC) Request Coordinator, Code 633.4, NASA/Goddard Space Flight Center, Greenbelt, MD 20771; Phone (301) 286-6695. To obtain S-7 data and a user's guide contact Mary Alice Woerner, MS 423, Data Management Office, NASA/Langley Research Center, Hampton, VA 23681; Phone (804) 864-5607.

REFERENCES

Auer, L. H., and K., Ch.-Y. Jim, 1991: Further analysis of the global outgoing longwave radiative flux observed by nimbus. *J. Geophys. Res.*, **96,** 17 367–17 370.

Barkstrom, B. R., 1984: The Earth Radiation Budget Experiment (ERBE). *Bull. Amer. Meteor. Soc.*, **65,** 1170–1185.

——, and G. L. Smith, 1986: The Earth Radiation Budget Experiment: Science and implementation. *Rev. Geophys.*, **24,** 379–390.

Bess, T. D., and G. L. Smith, 1987a: Atlas of wide-field-of-view outgoing longwave radiation derived from Nimbus 6 Earth Radiation Budget data set—July 1975 to June 1978. NASA RP-1 1185, 78 pp.

——, and ——, 1987b: Atlas of wide-field-of-view outgoing longwave radiation derived from Nimbus 7 Earth Radiation Budget data set—November 1978 to October 1985. NASA RP-1186, 174 pp.

——, and ——, 1991: Atlas of wide-field-of-view outgoing longwave radiation derived from Nimbus 7 Earth Radiation Budget data set—November 1985 to October 1987. NASA RP-1261, 52 pp.

——, ——, and T. P. Charlock, 1989: A 10-year monthly data set of outgoing longwave radiation from *Nimbus-6* and *Nimbus-7* satellites. *Bull. Amer. Meteor. Soc.*, **70,** 480–489.

Fein, J. S., and P. L. Stephens, 1987: *Monsoons.* John Wiley & Sons, 632 pp.

Green, R. N., 1983: Accuracy and resolution of earth radiation budget measurements. *J. Atmos. Sci.*, **40,** 977–985.

——, F. B. House, P. W. Stackhouse, X. Wu, S. A. Ackerman, W. L. Smith, and M. J. Johnson, 1990: Intercomparison of scanner and nonscanner measurements for the Earth Radiation Budget Experiment. *J. Geophys Res,* **95,** 11 785–11 798.

Harrison, E. F., D. R. Brooks, P. Minnis, B. A. Wielicki, W. F. Staylor, G. G. Gibson, D. F. Young, F. M. Denn, and ERBE Science Team, 1988: First estimates of diurnal variation of longwave radiation from the multiple-satellite Earth Radiation Budget Experiment (ERBE). *Bull. Amer. Meteor. Soc.*, **69,** 1144–1151.

Jacobowitz, H., H. V. Soule, H. L. Kyle, F. B. House, and the *Nimbus-7* ERB Experiment Team, 1984: The Earth Radiation Budget (ERB) Experiment: An overview. *J. Geophys. Res.*, **89,** 5021–5038.

Kyle, H. L., A. Mecherikunnel, P. A. Ardanuy, L. Penn, B. Groveman, G. G. Campbell, and T. H. Vonder Harr, 1990: A comparison of two major earth radiation budget data sets. *J. Geophys. Res.*, **95,** 9951–9970.

Smith, G. L., and T. D. Bess, 1983: Annual cycle and spatial spectra of earth-emitted radiation at large scales. *J. Atmos. Sci.*, **40,** 998–1015.

——, and R. N. Green, 1981: Deconvolution of wide field-of-view radiometer measurements of earth-emitted radiation. Part I: Theory. *J. Atmos. Sci.*, **38,** 461–473.

——, ——, E. Raschke, L. M. Avis, J. T. Suttles, B. A. Wielicki, and R. Davies, 1986: Inversion methods for satellite studies of the earth's radiation budget: Development of algorithms for the ERBE mission. *Rev. Geophys.*, **24,** 407–421.

Smith, W. L., J. Hickey, H. B. Howell, H. Jacobowitz, D. T. Hilleary, and A. J. Drummond, 1977: *Nimbus-6* Earth Radiation Budget Experiment. *Appl. Opt.*, **16,** 306–318.